

September 10, 2003

NoRH and *RHESSI* observations of the X 1.5 flare of April 21, 2002

M. R. Kundu¹, V. I. Garaimov¹, S. M. White¹, & S. Krucker²

¹*Astronomy Department, University of Maryland, College Park, MD 20742*

²*Space Sciences Laboratory, University of California, Berkeley CA 94720-7450*

kundu, gvi, white@astro.umd.edu

ABSTRACT

We present an overview of the radio observations of the X1.5 flare of April 21, 2002, and complementary data from other wavelengths. This flare was fairly well observed by the Ramaty High Energy Spectroscopic Imager (*RHESSI*) spacecraft and fully observed by the Nobeyama Radioheliograph (NoRH) at 17 and 34 GHz. This long-duration event lasted more than 2 hours and features a beautiful arcade of rising loops on the limb visible at X-ray, EUV and radio wavelengths. The main flare was preceded by a small event 90 minutes earlier showing a long EUV loop connecting well-separated radio and hard X-ray sources. The main flare itself starts with a compact radio and hard X-ray source at the eastern end of the region that develops into emission close to the solar surface (and well inside the solar limb) over a large region to the northwest. As the flare proceeds a large set of loops is seen to rise well above the solar limb. Distinct regions of radio emission with very different time behaviour can be identified in the radio images, and in particular a peculiar nonthermal source seen in radio and hard X-rays low in the corona at the base of the arcade is seen to turn on 30 minutes after the start of the impulsive phase. At about the same time an extremely intense burst of coherent radio emission is seen from 500 to 2000 MHz: we speculate that this lower-frequency burst is produced by electrons that are accelerated in the nonthermal source at the base of the arcade and injected into the loop system where they radiate plasma emission in the 10^{10} cm^{-3} density plasma at the top of the arcade of loops. This event is striking as a demonstration of the many ways in which a flare can produce radio emission, and the combined data at different wavelengths reveal a diversity of energy release and nonthermal acceleration sites.

Subject headings: Sun: flares – Sun: corona – Sun: radio radiation

1. INTRODUCTION

The Nobeyama Radioheliograph (NoRH) has been operating as a solar dedicated imaging instrument at 17 and 34 GHz since 1992. The new space mission, *Ramaty High Energy Spectroscopic Imager (RHESSI)*, has been operating since Feb. 2002. Both instruments produce images of sources of nonthermal electrons (e.g. solar flares) in the same energy range, but at two different wavelength regions. Hard X-rays (HXR) are produced by bremsstrahlung and microwave emission by gyrosynchrotron radiation of nonthermal electrons with energies in excess of 100 keV. Because the emission mechanisms are different, the two instruments offer information on different aspects of conditions in the corona, where such energetic electrons are produced. Hard X-rays are produced by bremsstrahlung, that is by collisions of energetic electrons with matter of high density; in general hard X-rays above 50 keV arise from nonthermal electrons striking the chromosphere, which is observed in X-ray images showing the foot points in coronal loops, where the accelerated electrons precipitate. Microwave emission from flares is produced by gyrosynchrotron radiation of 100's of keV electrons generated and subsequently accelerated in the flare energy release process. It turns out that this mechanism is very efficient and we are able to detect very high energy electrons even in very small flares. By contrast, flares in which X-rays above 100 keV can be imaged are rare because the steeply falling power law spectra do not yield sufficient photons at high energies for image formation.

In the past, comparisons of hard X-ray and microwave images involved hard X-rays below 32 keV during the SMM period and below 90 keV during the *Yohkoh* period. The sources of such hard X-rays are dominated by electrons whose energies are much lower than those that typically produce the nonthermal microwave emission. Early comparison of radio and hard X-ray images were done by Hoyng et al. (1983) and Kundu (1984). It seems that the two populations of nonthermal electrons may have different energy spectra, which implies that they may have different origins (e.g., Kundu et al. 1994; Silva et al. 2000). Detailed comparisons of microwave and hard X-ray images in 25 flares (Nobeyama and *Yohkoh* data) have been carried out by Nishio et al. (1997) and Nishio et al. (2000), who presented a scenario of flare energy release in which interaction of an emerging new loop with an overlying/existing loop structure is involved. In most cases, hard X-rays seem to come from loop foot points. In some cases microwave sources are also located at one or more foot points or legs of loops, and in other cases the entire coronal loop is involved in emitting microwave emission. This overall picture of relative positions of microwave and hard X-ray sources has been confirmed by other studies (e.g., Kundu et al. 1995; Gopalswamy et al. 1995; Hanaoka 1999; Kundu et al. 2001).

As mentioned earlier, *RHESSI* has been operating since February 2002 and collecting excellent data which permit us to produce hard X-ray images above 50 keV, and compare them with simultaneous microwave images of nonthermal electrons that produce high energy photons. In

this paper, we present an overview of the radio observations of the well-observed X1.5 class flare observed on April 21, 2002, and the results of a comparison of microwave images as obtained with NoRH at 17 and 34 GHz with *RHESSI* hard X-ray images in the energy ranges 6-300 keV.

2. OBSERVATIONS

This flare of GOES soft X-ray importance X1.5 occurred on April 21, 2002 near the limb at S14W84. It was fairly well observed by the spacecraft *RHESSI* and fully observed by the imaging telescope NoRH at 17 and 34 GHz and by the Nobeyama radio polarimeters at 1.0, 2.0, 3.75, 9.4, 17 and 35 GHz. High frequency radio and hard X-ray time profiles for the initial part of the event are presented in Figure 1. This is a long duration event (more than 2 hours). The radio and hard X-ray time profiles show several spikes during the rising phase with durations of order a minute. The *RHESSI* and *Transition Region And Coronal Explorer (TRACE)* observations of this event have been summarized by Gallagher et al. (2002). They report the initial activity seen in AR 9906 starting as early as 23:00 UT on April 20, 2002, with an impulsive soft X-ray spike peaking at 23:27 UT. We therefore produced NoRH images starting from 23:00 UT. The images were produced in the AIPS package with resolutions of 12'' at 17 GHz and 8'' at 34 GHz.

2.1. Preflare Event at 23:26 UT, April 20

Figure 2 shows observations of the preflare event at 23:27 UT. The radio and hard X-ray light curves match each other fairly well, but the images show a stark difference: the hard X-ray source is extremely compact and lies right at the limb, whereas the radio source lies inside the limb at the location where the April 21 flare subsequently starts (Gallagher et al. describe the location of the hard X-ray source as the same location as the start of the April 21 flare, but we disagree since as far as we know none of the hard X-ray images of the subsequent flare show X-rays in this limb location). Following this small event the preflare radio images show predominantly thermal bremsstrahlung emission from hot gas in the corona above the active region, although the brightest source, and the only circularly polarized source, is associated with a sunspot inside the limb and is probably weak gyroresonance emission. The circular polarization source is extended east-west. An interesting feature of this active region is the radio emission protruding well above the limb to the north-west of the region. A sequence of images indicates that this feature is time variable and shows outward motions; the sequence of *TRACE* 195 Å images also shows sporadic ejections of material in this location.

As noted by Gallagher et al. (2002), the hard X-rays in the April 20 23:26 UT event come

from a location right on the limb that is at the base of the extended coronal radio emission and EUV ejecta. This event is one of the most compact events seen by *RHESSI* and whether the proximity to the limb plays a role in its small size is not clear. Despite the good match of the radio and hard X-ray light curves, the flare radio emission comes from a location completely different from that of the hard X-rays, just to the north-east of the sunspot radio source that is polarized in the steady active region emission. Remarkably the *TRACE* 195 Å difference image (postflare minus preflare) shows a faint large loop connecting these two locations. This loop is a negative feature: it was present prior to the flare but not after the flare. A more careful inspection of the *TRACE* images shows that the loop emission was present at least 30 minutes prior to the flare and fades over the preflare period. This fading might not be related to the event at 23:26 UT, but the presence of the loop before the event does establish a magnetic connection between the sites of the radio and hard X-ray emission. Thus if one looks at only the radio data or only the hard X-ray data for this event one has completely the wrong impression that this was a very compact source at either the limb (X-ray) or the sunspot (radio), whereas in fact the combination of all three wavelengths clearly indicates that energy is released in a long structure connecting the two sites. There is insufficient data to determine whether the same population of electrons produces both radio and X-rays: the radio event is shorter than the X-ray event, but the radio emission may come from electrons more energetic than those that *RHESSI* can detect in this small event.

Note that the loop visible in the *TRACE* images connecting the radio and hard X-ray flare sites arches over virtually the entire volume subsequently occupied by the April 21 flare, but curiously its orientation (roughly east–west) is orthogonal to that of the loops in the post–flare arcade (north–south) observed above the limb two hours later.

2.2. Subsequent Preflare Activity (23:40 - 01:10 UT)

Because of the complex nature of this event and the availability of excellent data at a number of different wavelengths, a single set of images cannot convey the necessary information and so we present three figures showing the morphological evolution at EUV, radio and hard X-ray wavelengths. We compare one radio wavelength, one hard X-ray energy band and one EUV band (195 Å Fe XII/XXIV images) in Figure 3, focussing on the preflare period. Figure 4 shows the radio evolution of the flare via superpositions of 17 and 34 GHz radio contours on *TRACE* 195 Å images, and Figure 5 shows the hard X-ray evolution of the flare via hard X-ray contours for the 6–12, 12–25 and 25–50 keV photon energy bands overlaid on *TRACE* images at the same times as in Fig. 4.

As can be seen in Fig. 2, the preflare steady radio emission shows several components: the coronal emission feature protruding above the limb, the bright polarized source located over the

sunspot at the eastern end of the region, and emission bridging these two locations. From 00:16 to 00:38 UT the radio emission from the pre-flare region changes only slowly. The first detectable hard X-ray emission at 6–12 keV occurs near the radio sunspot source at about 00:40 UT (Figure 3a), well before the main rise of the flare. This *RHESSI* source location is close to the location of the later main radio flare source (labelled “Main src” in Fig. 3d). By 00:46 UT (Fig. 3c) one sees a single strong hard X-ray source coincident with the brightest 17 GHz radio emission, as well as a radio source at the limb (labelled “Limb src” in Fig. 3c) at the base of the EUV ejections remarked on earlier. However, there is little change in the 195 Å Fe XII image. The radio and hard X-ray sources gradually brighten with time and by 00:58 UT (Fig. 3d) the 195 Å image is also showing quite bright emission coincident with the brightest radio and hard X-ray emission. After 01:00 UT the rise in fluxes towards the flare peak begins and the images show emission over a larger volume, filling in the region between the main and the limb radio sources. The 195 Å image starts to show diffuse emission above the limb, indicated by the arrow in Fig. 3e, that we attribute to the Fe XXIV line within the *TRACE* 195 Å passband (Fig. 3e), and by 01:07 UT (Fig. 3f) the 6–12 keV hard X-rays also peak above the limb while the radio emission continues to peak inside the limb.

The preflare radio images in Figure 4 indicate that the 34 GHz emission closely resembles the 17 GHz emission. Images in the different hard X-ray energy ranges also show general similarity in the preflare period (Figs. 5a-b). At about 00:46 UT the *RHESSI* source at higher energies (25–50 keV) appears elongated (Fig. 5a), suggesting that it looks like a compact loop with components at the two ends of the loop. At the same time the 6–12 and 12–25 keV emission appears to be located at the west end of this loop. Gallagher et al. (2003) note that the *TRACE* images show a faint diffuse feature that might represent the onset of the associated coronal mass ejection erupting above the whole active region starting at about 00:50 UT, but this faint feature is not emphasized by the intensity representation in our figures. At 00:58 UT (Fig. 5b) the 12–25 and 25–50 keV hard X-ray images both show emission extended east–west, with the lower energy 6–12 keV hard X-ray source lying between them, as expected if the higher energy HXR come from footpoints of a loop while the softer X-rays come from the top of the loop. This pattern continues until about 01:02 UT, when a strong compact 17 GHz source (labelled “NW src” in Fig. 4c) appears to the north–west of the main 17 GHz source but not quite coincident with the earlier limb source (compare Figs. 3c and 3d).

2.3. The Main Flare

The main flare (April 21, 2002) started at about 01:08 UT with a steep rise in the radio and hard X-ray fluxes. The time profile from NoRH shows several sharp peaks at both 17 and 34 GHz, starting at 01:11 and continuing until 02:25 (see Figs. 1 & 7). These peaks coincide in time at

17 and 34 GHz. The last two peaks are not spiky, but are rather smooth and broad. *RHESSI* maps at short cadence are available only until about 01:30 UT when *RHESSI* enters nighttime. The time profiles of the NoRH radio data and *RHESSI* hard X-ray data show that there is good correspondence between the peaks observed at 17 GHz and the peaks observed in the *RHESSI* energy channels above 25 keV until 01:30 UT.

The high frequency radio spectral index during the impulsive phase is in the range -2.5 to -2 , corresponding to an electron energy power law with a nonthermal spectral index of -4 to -3.5 . From the hard X-ray data Gallagher et al. (2002) find energy spectral indices during the impulsive phase of order -3.2 , i.e., slightly flatter than we infer from the radio data. However, given the diverse range of structures exhibited by this flare, a single value for the spectral index probably does not represent all the emission present at either radio or X-ray wavelengths.

From 01:05 UT onwards the two prominent microwave peaks intensify and beginning at 01:08 UT the lower intensity radio contours outline a large volume that essentially corresponds to the volume under the arcade of loops visible in the *TRACE* 195 Å images (Figs. 4c-f). Between 01:08 and 01:13 UT the 25–50 keV images are of poor quality and we omit the corresponding contours from Fig. 5c. The *RHESSI* images in the lower energy channels from this time onwards no longer show emission from the main flare source inside the limb, but rather are dominated by emission from the top of the rising arcade of EUV loops (Fig. 5c-f). The apparent lack of emission at photon energies below 25 keV from inside the limb may simply be due to dynamic range effects in the *RHESSI* images: given the complex spatial structure of this flare there may not be sufficient dynamic range in the *RHESSI* images to see weaker emission inside the limb in the presence of the very bright emission from hot thermal plasma at the top of the arcade of loops.

At higher photon energies the looptop emission is weak and the images again clearly show emission sources inside the limb. The two prominent microwave sources visible at both 17 and 34 GHz (Fig. 4c,d) both have clear counterparts in the 25–50 keV images from 01:13 UT onwards (Fig. 5d,e). It is not clear whether these two hard X-ray sources are footpoints of a loop structure or are independent bright regions of precipitation of nonthermal electrons. The dominance of the two sources inside the limb in the microwave and > 25 keV hard X-ray images continues until about 01:20 UT when the northwestern of the two bright microwave sources becomes dominant (Fig. 4e). From 01:20 onwards, we see again compact HXR foot point sources inside the limb as well as 12–25 keV and 25–50 keV emission from the tops of the loops overlying these footpoints. Note that the radio and hard X-ray footpoints are not symmetric: in hard X-rays the southern footpoint is generally brighter, while in radio the northern footpoint is brighter.

The morphology of the NoRH source structure changes considerably during the period 01:30–02:30 UT. Figure 6 shows *TRACE* images with superimposed radio contours at different times (01:35, 02:09, 02:30, and 02:59 UT) and hard X-ray contours at 02:09 and 02:30 UT when *RHESSI*

can again see the Sun. Initially the radio emission is brightest in the two sources close to the surface discussed above (labelled the “Main src” and “NW src” sources in Fig. 4c) whereas the outer contours seem to outline the area visible in the *TRACE* images as diffuse emission, attributed to Fe XXIV line emission within the 195 Å passband from the hot soft X-ray-emitting loops that lie above the cooler loops emitting the Fe XII line. The whole source grows in size with time. Starting at about 01:40 UT we see radio emission from the region of the main flare source begin to strengthen. This radio source (labelled “M” in Fig. 6b) has a nonthermal radio spectrum and grows in intensity and size with time, and by 02:00 it is easily the brightest source of radio emission, dominating the eastern side of the radio source; directly above it (in the radial direction) lies another bright feature at the height of the arcade of *TRACE* loops (labelled “SW” in Fig. 6b), which the radio spectrum shows is also nonthermal. However the outermost radio contours to the north in Fig. 6b coincide with the beautiful arch system in the *TRACE* images, and the radio spectrum of this emission is flat, implying that it is thermal bremsstrahlung from the cooler gas radiating the Fe XII line.

As time proceeds the nonthermal radio sources “M” and “SW” strengthen relative to the thermal emission from the *TRACE* loops and at 02:30 the nonthermal sources dominate the radio images. *RHESSI* emerges from the Earth’s shadow at around 02:08 UT and is then able to continue imaging the flare. The last 2 panels in Figure 6 show *RHESSI* images at hard (30–100 keV) and soft (10–20 keV) X-ray photon energies. The soft X-ray images show emission coming predominantly from a large extended source above the arcade of loops that dominates the Fe XII image, consistent with a picture in which the higher loops are hotter because the energy release site moves to progressively higher altitudes with time (Gallagher et al. 2002). However, the 30–100 keV photons arise in a source that is essentially coincident with the nonthermal 17 GHz radio emission: initially at the base of the radio stalk (source “M” in Fig. 6b,f), which we infer to be close to the photosphere, and also at another location to the west in the 02:29:55 image (labelled “W” in Fig. 6f). We only see the position of the western 30–100 keV source W in projection onto the sky plane and so we do not know where along the line of sight it lies. This affects the height of the source relative to the solar surface that we infer and hence its interpretation: if source W is at the same longitude but lies radially above source M then its altitude is about 2×10^9 cm and it is a purely coronal source, in which case thick target emission would require a high density at that height; or else the source lies well to the west of source M in longitude, in which case it would be at a much lower altitude and could be consistent with thick target hard X-rays from a chromospheric location just inside the projected solar limb. The coincidence of the nonthermal 17 GHz and 30–100 keV hard X-ray sources in the extended phase confirms that in addition to the heating at large altitudes responsible for the soft X-ray emitting loops, energy release and particle acceleration also continue low in the solar atmosphere.

By 03:00 UT the nonthermal SW radio source at the height of the *TRACE* looptops has faded

and the thermal emission is again more pronounced in the radio images, but the nonthermal source M at the base of the arcade remains strong. The *RHESSI* data show that the softer hard X-rays (< 20 keV) continue to come from heights well above the *TRACE* 195 Å loops.

2.4. Lightcurves of individual sources

We have analyzed the 17 and 34 GHz light curves of four individual sources that can be distinguished in this event, shown in Figure 7. (1) The main source is the source close to the sunspot at the eastern end of the active region, where the flare starts: the brightest radio emission is located here throughout the flare except during the brightest peak (Fig. 1), discussed next. (2) As shown in Fig. 4e-f, during the impulsive phase (roughly the period 01:10 – 01:30 UT) the brightest radio emission actually comes from a region some $30''$ to the northwest (NW) of the main source. This NW source reaches a peak brightness temperature of 10^8 K at 01:24, but it decays very rapidly after 01:30 UT and is insignificant during the long decay phase of the event. (3) During the extended decay phase of the event a brightening is seen west–south–west of the main source, well above the solar limb at the south end of the arcade of loops seen in *TRACE* (compare the top two panels of Fig. 6). The spectrum shows that this source, like the main and northwest sources, is nonthermal, and its light curve is similar to that of the main source until 02:30 UT. (4) The emission from the tops of the loops in the arcade to the north of the main source is confirmed by our analysis to be purely optically thin thermal bremsstrahlung, for which the brightness temperatures satisfy $T_{B,17} = 4T_{B,34}$. Since it has a brightness temperature of $1\text{--}2 \times 10^6$ K yet has a flat spectrum and hence is optically thin, the true temperature of this gas must lie in the soft X-ray range.

3. NONTHERMAL PROCESSES IN THE LOOP ARCADE

As noted above, nonthermal 17 GHz radio emission from the main and southwest sources is seen to continue long after the impulsive phase of the event. The main source takes on the appearance of a stalk of emission projecting vertically from a location close to the sunspot at the eastern end of the active region where the flare starts (source M in Fig. 7), and this stalk points at the southwest peak (Fig. 6b-d). This nonthermal stalk of radio emission starts to become prominent at around 01:45 UT. The low–frequency radio emission from this event also shows a dramatic feature starting at this time: a broadband continuum initially from 500–2500 MHz that forms an envelope drifting to lower frequencies with time (Figure 8) and terminating at about 02:45 UT. Such broadband flare–associated continua are usually referred to as “Type IV” bursts when observed at low frequencies. In Figure 9 we compare the lightcurve of the 1 GHz emission with the 17 GHz lightcurve from the main nonthermal source. The onsets of the two match extremely

well as do the times of decline. While details in the rest of the lightcurve match only in the gross sense, this is not too surprising given that the 1 GHz emission is coherent and hence is expected to fluctuate more wildly than the incoherent gyrosynchrotron emission at 17 GHz. For this reason we show the 1 GHz light curve in a logarithmic scale while the 17 GHz light curve is on a linear scale. The 30–100 keV light curve matches the structure of the 17 GHz emission from the nonthermal source once *RHESSI* can again observe the Sun after 02:10 UT (Fig. 9), confirming the link between the hard X-ray source and the nonthermal radio source found in the images. By contrast, the 10–20 keV light curve does not correlate with the 17 GHz emission, showing only a steady decline after 02:10 UT.

The 1 GHz emission reaches a flux of over 10^5 sfu and is 100% left circularly polarized according to the Nobeyama Radio Polarimeter (NoRP) data (it is the brightest 1 GHz burst reported by NoRP since 1993). The high polarization and broadband nature of the emission suggest plasma emission from nonthermal electrons trapped on loops with a range of densities: assuming second harmonic plasma emission, we require a density of $1.2 \times 10^{10} \text{ cm}^{-3}$ to explain plasma emission at 2 GHz. We argue that densities this high must be associated with the post-flare plasma trapped in the arcade of rising loops: such high densities are unlikely to be present on open field lines, which probably describes many of the field lines above the arcade. This fixes a size scale for the 1 GHz emission of about the length of the arcade, or $100''$: assuming a source area of order $5 \times 10^{19} \text{ cm}^2$, we infer a peak brightness temperature of over 10^{11} K , confirming the need for a coherent emission mechanism. From the similarity in onset times between the nonthermal stalk at 17 GHz and the high-frequency Type IV, we speculate that the electrons producing the 1 GHz plasma emission are in fact accelerated in the base of the stalk and injected into the loops making up the arcade above the stalk. If so, the true size of the 1 GHz source is probably smaller than we inferred above and the true brightness temperature even higher than 10^{11} K .

4. CONCLUSION

The 2002 April 21 X1.5 flare produced a range of radio emissions, from preflare activation over a large volume to compact nonthermal impulsive components, thermal emission from the arcade of rising loops and nonthermal emission in the extended phase from a peculiar source at the base of the arcade. While flare radio emission is seen from a large volume of the corona, many of the interesting features arise from close to the location of the precursor event at 23:26 UT which is also the location of the onset of the radio flare and the late-phase nonthermal source.

The energy distribution inferred for the radio-emitting electrons during the impulsive phase is quite similar to that inferred for the hard X-ray-emitting electrons, and the radio and hard X-ray light curves show similar time structure. In the radio images we can identify at least four

spatially distinct regions that show quite different temporal behaviour. The brightest radio emission in the flare comes from a location to the north–west of the location where the flare starts, under the middle of the loop arcade, but the radio emission from this location fades after the impulsive phase and is unimpressive during the extended decay phase. On the other hand, the main source and the thermal and nonthermal sources in the arcade all participate in the extended phase. The nonthermal radio and hard X–ray source that appears after 01:45 UT has no obvious counterpart at EUV wavelengths and coincides with the onset of a strong continuum burst in the 1 – 2 GHz range that is bright enough to disrupt cell phone communications (Nita et al. 2002).

This event is striking as a demonstration of the many ways in which a flare can produce radio emission, and the combined data at different wavelengths also reveal a diversity of energy release and nonthermal acceleration sites, starting with the east–west loop of the precursor event, the main flare site low in the corona, the heating in loops above the *TRACE* arcade after the impulsive phase shown by the *RHESSI* 6–12 keV images, and the long–lasting acceleration source at the base of the south end of the arcade seen in the radio and 30–100 keV hard X–ray images to be feeding nonthermal electrons into the arcade loops.

This research was supported by NSF grant ATM 99-90809 and NASA grants NAG 5-8192, NAG 5-10175, NAG 5-12860 and NAG 5-11872. We thank K. Hori for providing the HiRAS dynamic spectrum from the Hiraiso radio spectrograph (CRL, Japan) shown in Figure 8. We gratefully acknowledge the open-data policies of NoRH and the NASA satellites *RHESSI* and *TRACE* and their instrument teams which make multi-wavelength research such as this much easier. Alexander Nindos and the referee are thanked for their comments on the manuscript.

REFERENCES

- Gallagher, P. T., Dennis, B. R., Krucker, S., Schwartz, R. A., & Tolbert, A. K. 2002, *Solar Phys.*, 210, 341
- Gallagher, P. T., Lawrence, G. R., & Dennis, B. R. 2003, *Astrophys. J. (Lett.)*, 588, L53
- Gopalswamy, N., Raulin, J. P., Kundu, M., Nitta, N., Lemen, J. R., Herrmann, R., Zarro, D., & Kosugi, T. 1995, *Astrophys. J.*, 455, 715
- Hanaoka, Y. 1999, *Publ. Astron. Soc. Japan*, 51, 483
- Hoyng, P., Marsh, K. A., Zirin, H., & Dennis, B. R. 1983, *Astrophys. J.*, 268, 865
- Kundu, M. R. 1984, *Adv. Space Res.*, 4, 157
- Kundu, M. R., Nindos, A., White, S. M., & Grechnev, V. V. 2001, *Astrophys. J.*, 557, 880
- Kundu, M. R., Nitta, N., White, S. M., Shibasaki, K., Enome, S., Sakao, T., Kosugi, T., & Sakurai, T. 1995, *Astrophys. J.*, 454, 522
- Kundu, M. R., White, S. M., Gopalswamy, N., & Lim, J. 1994, *Astrophys. J. Supp.*, 90, 599
- Nishio, M., Kosugi, T., Yaji, K., Nakajima, H., & Sakurai, T. 2000, *Advances in Space Research*, 25, 1791
- Nishio, M., Yaji, K., Kosugi, T., Nakajima, H., & Sakurai, T. 1997, *Astrophys. J.*, 489, 976
- Nita, G. M., Gary, D. E., Lanzerotti, L. J., & Thomson, D. J. 2002, *Astrophys. J.*, 570, 423
- Silva, A. V. R., Wang, H., & Gary, D. E. 2000, *Astrophys. J.*, 545, 1116

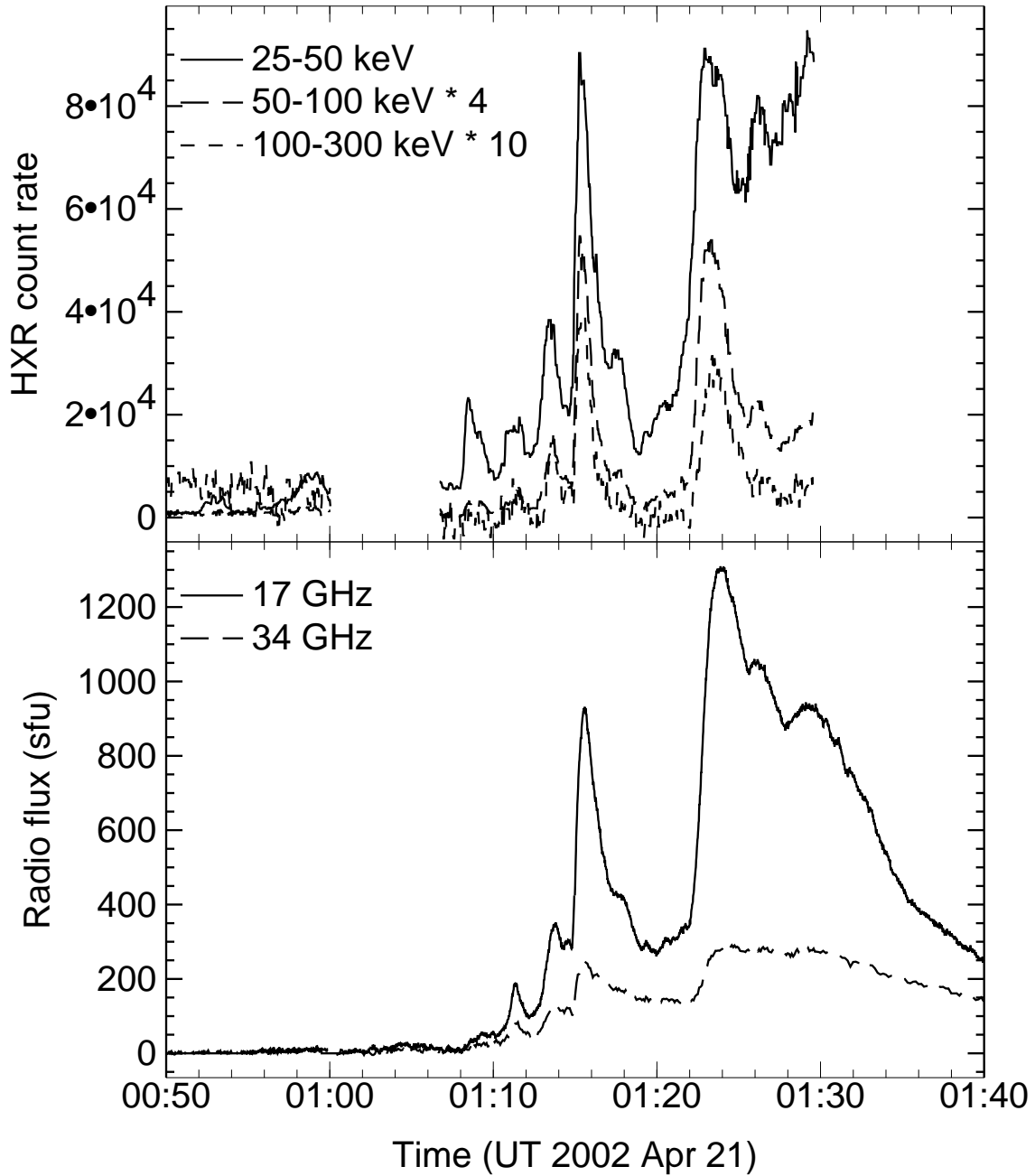


Fig. 1.— Hard X-ray (*RHESSI* 25–50, 50–100 and 100–300 keV) and radio (NoRP 17 GHz total flux and NoRH 34 GHz flux) lightcurves for the 2002 April 21 event. The hard X-rays have 4 s time resolution and the radio light curves (preflare subtracted) have 1 s resolution. The 50–100 and 100–300 keV light curves are multiplied by 4 and 10, respectively, for display purposes.

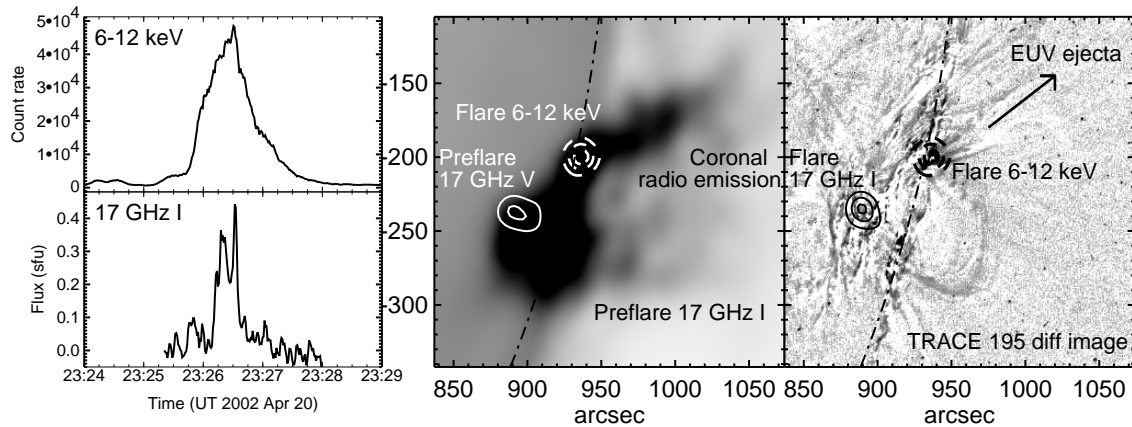


Fig. 2.— Radio and hard X-ray observations of the preflare event at 23:26 UT on April 20. The left panels show the 6–12 keV hard X-ray and 17 GHz radio total intensity light curves; the radio emission is approximately 60% right circularly polarized throughout the event. The middle panel shows the preflare radio image (greyscale: 17 GHz I, saturated at a brightness temperature of 35000 K; solid white contours: 17 GHz V) and for reference the location of the hard X-ray flare source (dashed white contours). The right panel shows a *TRACE* 195 Å difference image (mean over a 5 minute period after the flare minus the mean over 5 minutes prior to the flare) with the positions of the 17 GHz flare radio emission (solid contours, shown with the preflare image subtracted) and the hard X-rays (dashed contours) marked. The loop feature is negative, i.e., emission from the loop diminished at the time of the flare. The arrow on this panel indicates the direction of motion of the EUV ejecta (not visible in this image). All 17 GHz radio images in this paper are restored with a 12'' gaussian beam.

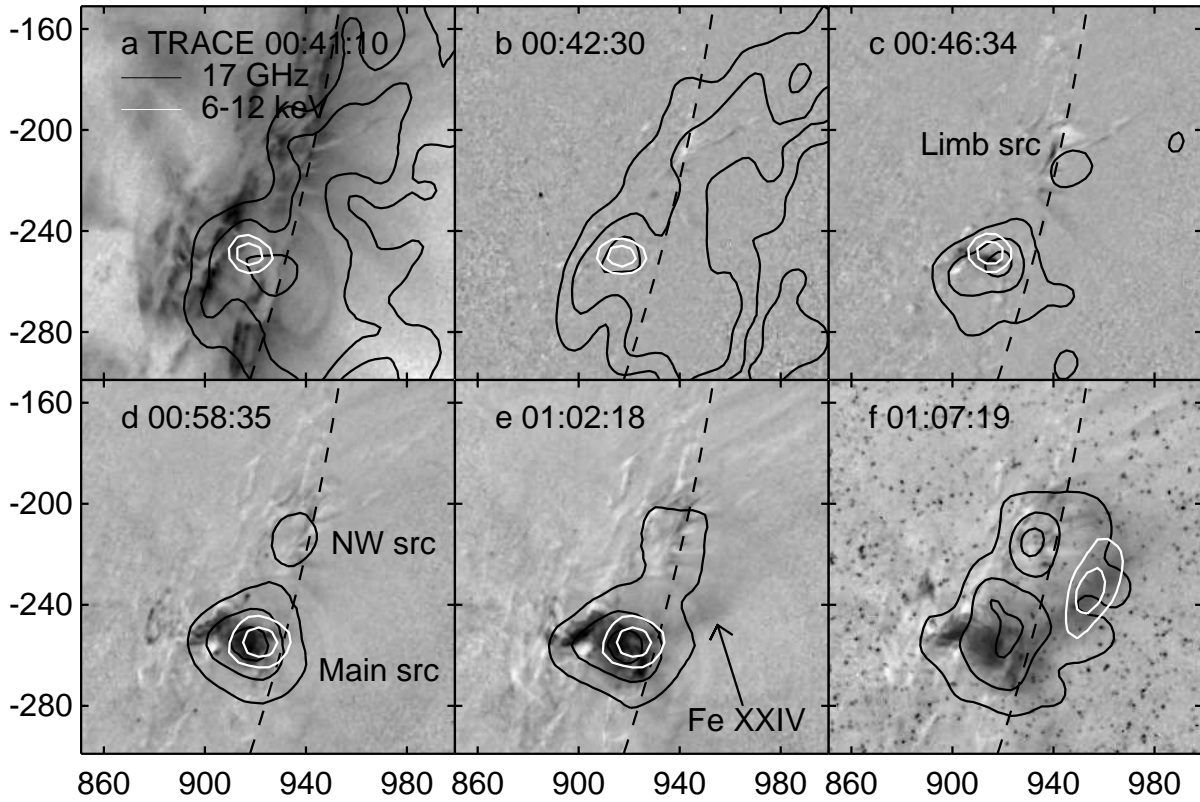


Fig. 3.— A sequence of overlays of 17 GHz radio (solid black contours) and 6-12 keV hard X-ray (solid white contours) images on *TRACE* 195 Å Fe XII images (with the color table reversed so that black indicates bright emission) during the long preflare period prior to the impulsive phase. In the last five panels the 195 Å image from the first panel has been subtracted in order to emphasize changes. The radio contours are at 10, 40 and 80% of the maximum in each image, while the 6–12 keV contours are at 30 and 70% of the maximum. Radio maxima at any time can be obtained from Figure 7. The EUV limb is shown by a dashed line in each panel and features referred to in the text are labelled.

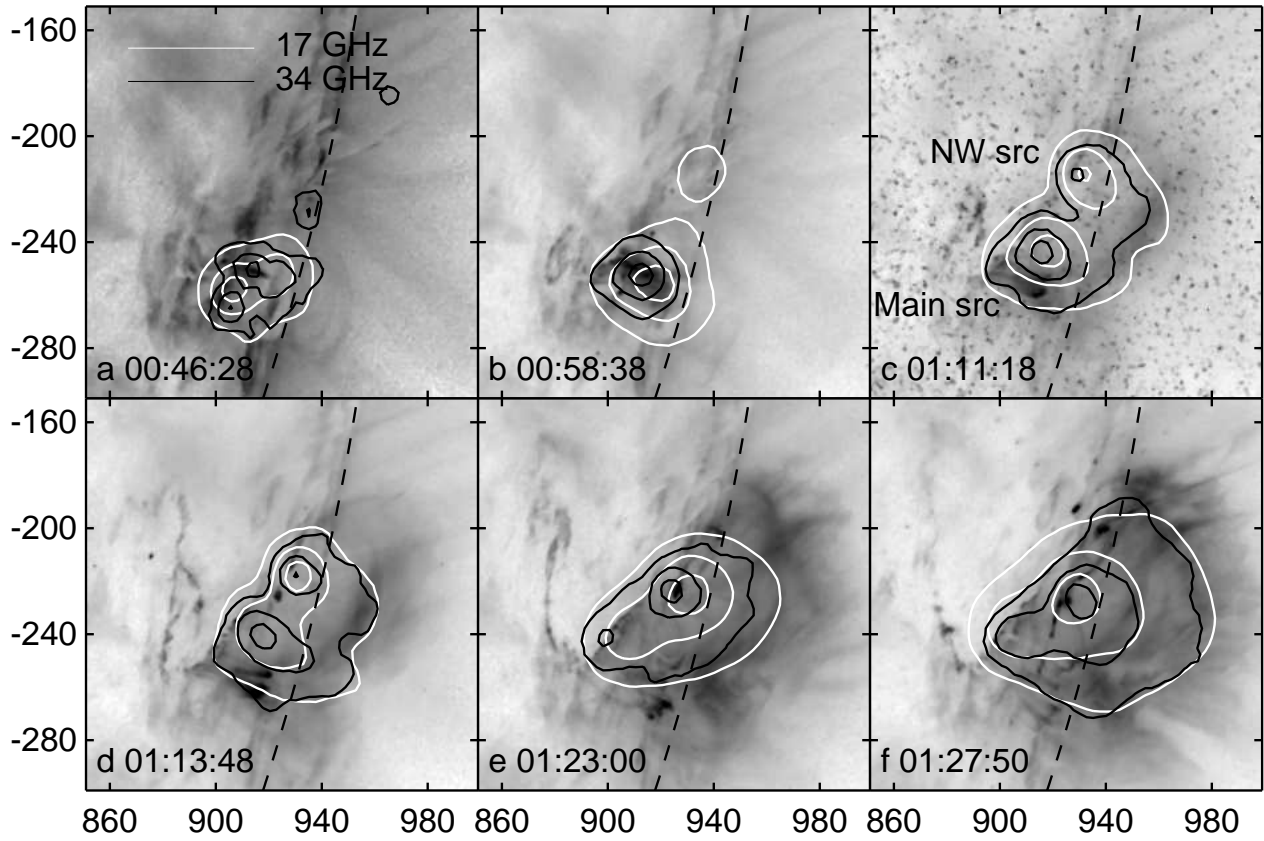


Fig. 4.— A sequence of overlays of 17 (white contours) and 34 (black contours) GHz images on *TRACE* 195 Å Fe XII images (inverted color table) during the main phase of the flare. Contour levels are at 10, 40 & 80% of the maximum in each image. The 17 GHz images have a 12'' beam and the 34 GHz images have an 8'' beam.

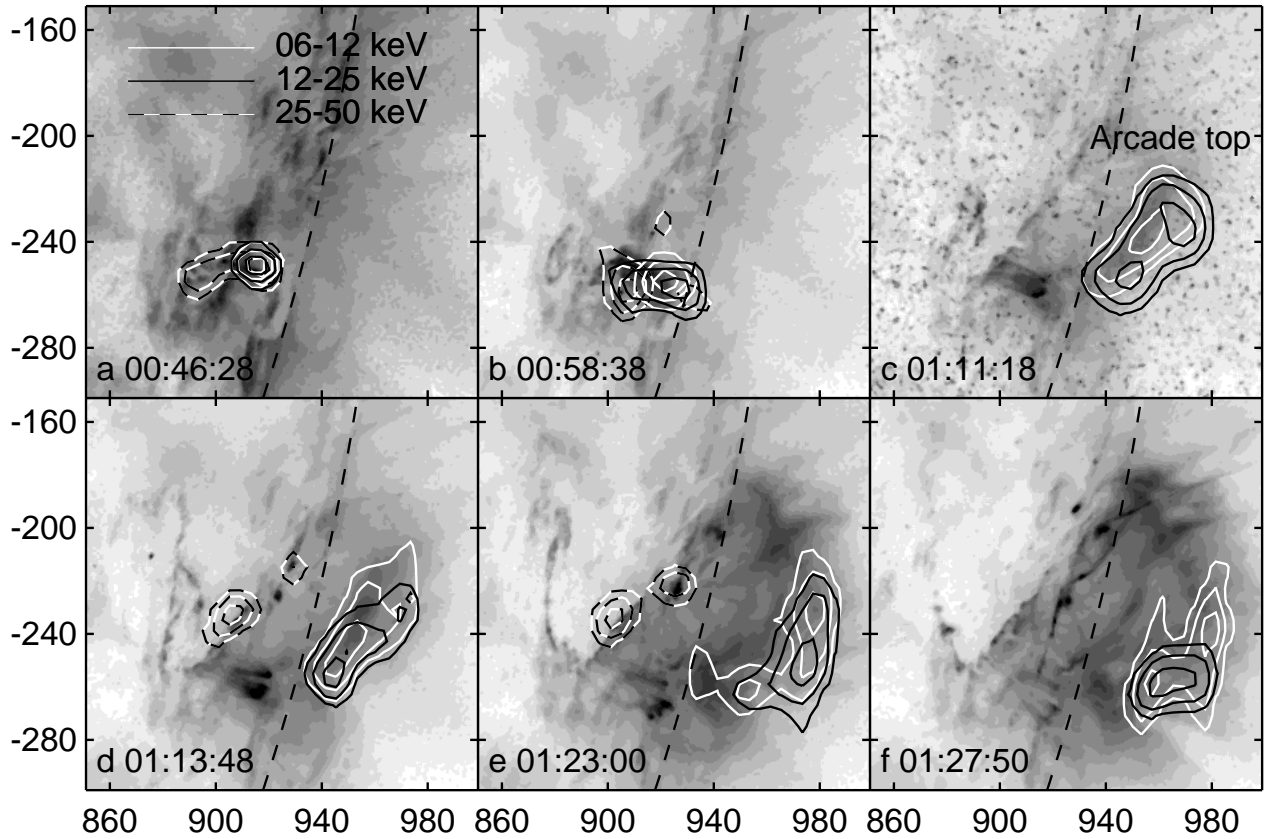


Fig. 5.— A sequence of overlays of *RHESSI* hard X-ray images on *TRACE* 195 Å Fe XII images (inverted color table) during the main phase of the flare. 6–12 keV images are shown in white contours, 12–25 keV images in black contours and 25–50 keV images in dashed contours. Contour levels are at 10, 40 & 80% of the maximum in each image. 12–25 keV contours are not shown at 01:11:18 (panel c) due to the poor quality of those images, and are not shown at 01:27:50 because severe pile-up at that time means that the 25–50 keV image may be dominated by photons of 12–15 keV.

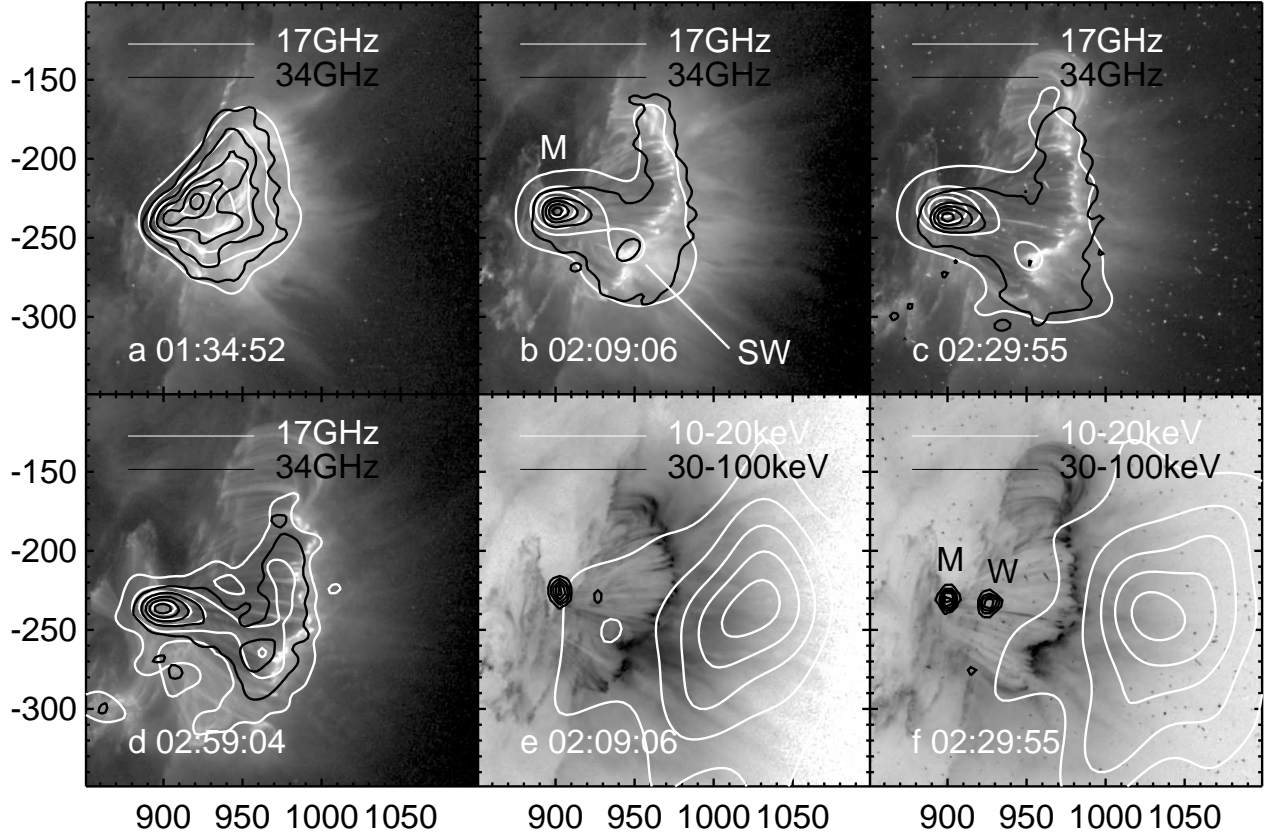


Fig. 6.— The evolution of the radio and hard X-ray sources later in the flare. The first four images show a sequence of overlays of 17 (white contours) and 34 (black contours) GHz images on *TRACE* 195 Å Fe XII images during the extended phase of the flare when the loop system is expanding above the west limb. The upper 4 contour levels are at 30, 50, 70 & 90% of the maximum in each image, while the lowest contour is at 10, 4, 2 & 10%, respectively, to match the changes in the peak intensity (see Fig. 7). *RHESSI* comes out of eclipse at 02:08, and the last two images show contours of the *RHESSI* 10–20 keV (white) and 30–100 keV (black) emission overlaid on the *TRACE* 195 Å Fe XII images at 02:09:56 and 02:29:55 (displayed with inverted color table). The prominent nonthermal radio source is visible at the eastern base of the radio source from 02:00 onwards. The radio emission from the loop tops at the northern end of the arcade has a flat spectrum and hence probably thermal free–free emission. The 10–20 keV hard X-rays originate above the EUV loops, in higher soft X-ray emitting loops, while the harder 30–100 keV X-rays originate at the same location as the nonthermal radio source.

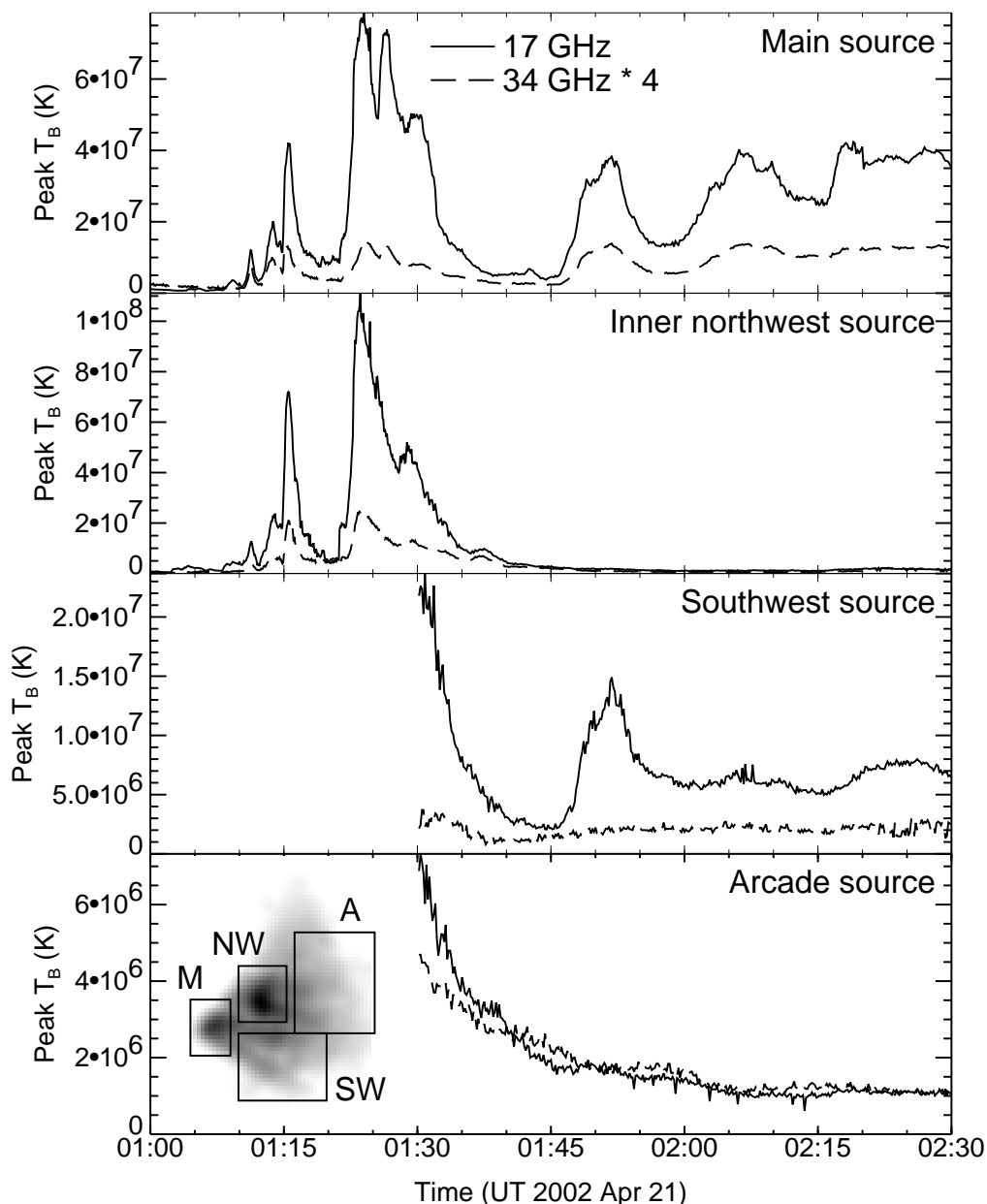


Fig. 7.— Peak brightness temperature versus time for sources in the four regions shown in the lower left (34 GHz image at 01:30:00). Essentially the sources are (a) the main source at the eastern end of the active region, which is the brightest source except during the impulsive phase; (b) the brightest source in the region just to the north-west of the main source, which is brightest source in the impulsive phase; (c) the brightest source to the southwest of the main source, where a nonthermal brightening is seen late in the event; and (d) the brightest source in the top of the arcade of rising loops seen in *TRACE* 195 Å images. We plot peak 17 GHz brightness temperature T_B and 4 times the peak 34 GHz T_B : for a thermal bremsstrahlung source these two should be the same, as they are in the loop arcade. The southwest and arcade sources are only present after the impulsive phase, so we only plot them after 01:30 UT.

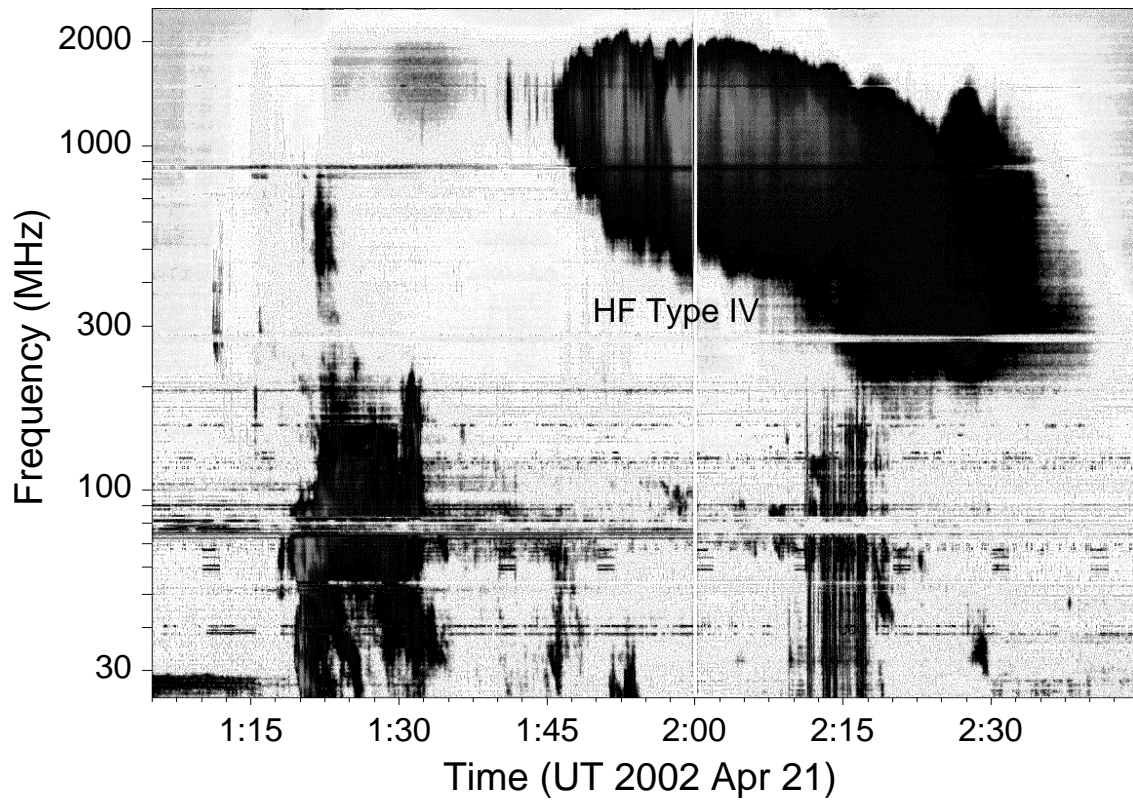


Fig. 8.— The dynamic spectrum of the event from 25 to 2500 MHz observed by the Hiraiso spectrograph. The strong broadband emission after 01:45 from 500–2000 MHz that we call “high-frequency Type IV” (“HF Type IV”) is labelled.

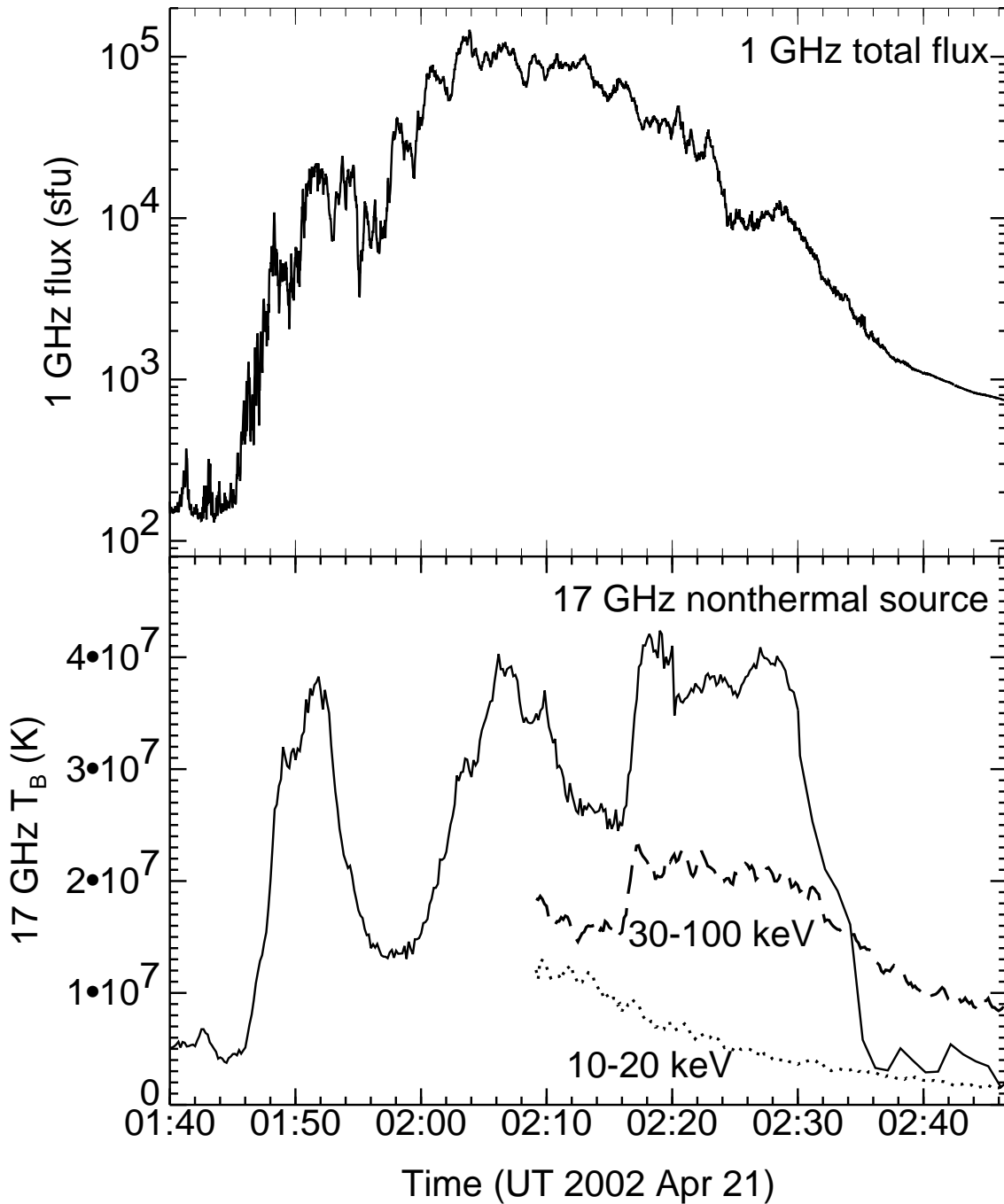


Fig. 9.— A comparison of the 1 GHz total flux (from NoRP data) and the 17 GHz peak brightness temperature light curve for the main source after 01:40 UT. The 1 GHz data are shown on a logarithmic scale while the 17 GHz and hard X-ray data are on a linear scale: the 1 GHz emission is coherent while the 17 GHz is incoherent, so the 1 GHz data are expected to fluctuate more. In the lower panel the 10–20 keV (dotted line, multiplied by 600) and 30–100 keV (dashed line, multiplied by 60000) *RHESSI* photon count rates are shown after 02:08 when *RHESSI* is again viewing the Sun.